

TAM receptors regulate multiple features of microglial physiology

Lawrence Fourgeaud^{1*}, Paqui G. Través^{1,2*}, Yusuf Tufail³, Humberto Leal-Bailey^{1,4}, Erin D. Lew¹, Patrick G. Burrola¹, Perri Callaway¹, Anna Zagórska¹, Carla V. Rothlin⁵, Axel Nimmerjahn³ & Greg Lemke^{1,6}

Microglia are damage sensors for the central nervous system (CNS), and the phagocytes responsible for routine non-inflammatory clearance of dead brain cells¹. Here we show that the TAM receptor tyrosine kinases Mer and Axl² regulate these microglial functions. We find that adult mice deficient in microglial Mer and Axl exhibit a marked accumulation of apoptotic cells specifically in neurogenic regions of the CNS, and that microglial phagocytosis of the apoptotic cells generated during adult neurogenesis^{3,4} is normally driven by both TAM receptor ligands Gas6 and protein S⁵. Using live two-photon imaging, we demonstrate that the microglial response to brain damage is also TAM-regulated, as TAM-deficient microglia display reduced process motility and delayed convergence to sites of injury. Finally, we show that microglial expression of Axl is prominently upregulated in the inflammatory environment that develops in a mouse model of Parkinson's disease⁶. Together, these results establish TAM receptors as both controllers of microglial physiology and potential targets for therapeutic intervention in CNS disease.

Microglia, the tissue macrophages of the brain and spinal cord, have fundamental roles in CNS homeostasis. They are mobilized in response to nearly any CNS perturbation, and can act to both resolve and exacerbate CNS disease¹⁷. Their importance notwithstanding, the signalling systems that regulate microglial function are only beginning to be deciphered. We asked whether the TAM receptor tyrosine kinases might comprise one such system. These receptors, Tyro3, Axl, and Mer, regulate the innate immune response in dendritic cells and macrophages^{2,8,9}, mediate the engulfment of apoptotic cells by phagocytes^{10–12}, promote the infection of cells by enveloped viruses¹³, and contribute to the growth and metastasis of human cancers¹⁴. In the CNS, Tyro3 is abundant in neurons^{15,16}, whereas Mer and Axl are present in microglia^{17–19}.

Microglia express the fractalkine receptor Cx3cr1 and the ionized calcium-binding adaptor Iba1^{20,21}. We therefore used Mer, Axl, glial fibrillary acidic protein (GFAP), and S100b antibodies to stain brain sections from Cx3cr1^{GFP/+} and S100b^{GFP/+} adult mice, which express GFP in microglia and astrocytes, respectively²² (see Methods). Mer co-localized with GFP⁺ microglia and not with GFAP⁺ astrocytes or S100b⁺ cells in Cx3cr1^{GFP/+} mice (Extended Data Fig. 1a, b); and with Iba1 in wild-type and S100b^{GFP/+} mice (Extended Data Fig. 1c). We do not exclude Mer expression in adult astrocytes (as seen for neonatal astrocytes²³) at levels below immunohistochemical detection, but microglia abundantly express *Mertk* mRNA¹⁷, and Mer plus CD64 is now the definitive marker pair for all tissue macrophages¹⁷. We detected only low Axl expression in the CNS. As shown below, this expression is elevated in inflammatory environments.

The best-studied role for TAM receptors is in the phagocytic clearance of apoptotic cells^{2,10–12}. We therefore asked if Mer and Axl

were required for clearance of the apoptotic cells generated during adult neurogenesis, which occurs in the subgranular zone of the dentate gyrus and the subventricular zone (SVZ) abutting the lateral ventricle, and produces neurons that integrate into the hippocampus and olfactory bulb, respectively³. We used the CLARITY imaging method with Cx3cr1^{GFP/+} mice to show that the SVZ, like the rest of the CNS¹, is tiled by microglia (see Supplementary Video 1). During neurogenesis in the mouse subgranular zone, ~80% of cells die within 8 days of their birth⁴. These dead cells are rapidly cleared by microglia, such that apoptotic cells are difficult to detect in a healthy brain⁴. Indeed, when we examined SVZ sections from Cx3cr1^{GFP/+} brains using cleaved caspase 3 (cCasp3) as a marker of apoptotic cells⁵, we were unable to detect even a single cCasp3⁺ cell in many sections (Fig. 1a). In marked contrast, the SVZ from Axl^{-/-}Mertk^{-/-}Cx3cr1^{GFP/+} mice was studded with cCasp3⁺ cells (Fig. 1a), which were negative for the neuronal marker NeuN (Fig. 1a). Uncleared apoptotic cells extended into the Axl^{-/-}Mertk^{-/-} rostral migratory stream (RMS), the pathway through which newborn cells migrate to the olfactory bulb (Fig. 1b). Apoptotic cells were confined to Axl^{-/-}Mertk^{-/-} neurogenic regions, however, and were not seen elsewhere in the CNS (Extended Data Fig. 2). Microglia in the Axl^{-/-}Mertk^{-/-} SVZ and RMS displayed elevated expression of GFP (controlled by the Cx3cr1 promoter), Iba1, and Siglec-1 (CD169), as well as an 'activated amoeboid' morphology¹ (Fig. 1a, c).

Consistent with the minimal expression of Axl, no accumulation of apoptotic cells was detected in the Axl^{-/-} SVZ (Extended Data Fig. 3a). In contrast, the Mertk^{-/-} SVZ contained many cCasp3⁺ apoptotic cells, although this number was around fourfold lower than that seen in Axl^{-/-}Mertk^{-/-} double mutants (Extended Data Fig. 3a). We counted 733 ± 359 (± s.e.m.) cCasp3⁺ cells per mm² in sections of the Mertk^{-/-} SVZ, and 2942 ± 262 cCasp3⁺ cells per mm² in the Axl^{-/-}Mertk^{-/-} SVZ. This synergistic effect of an Axl mutation on the background of an existing Mertk mutation has been noted previously^{2,5,8,9,12}.

We demonstrated that accumulation of apoptotic cells in the Mertk^{-/-} SVZ and RMS is due to the loss of Mer specifically from microglia, by analysing a new mouse line carrying conditional floxed alleles of the *Mertk* gene (Extended Data Fig. 4; see Methods) crossed to a tamoxifen-inducible oestrogen receptor (ER) Cre driver controlled by the Cx3cr1 promoter²⁴. In the absence of tamoxifen (upon vehicle injection alone), Mer was present in Cx3cr1^{CreER/+}Mertk^{fl/fl} Iba1⁺ microglia (Extended Data Fig. 5a), and there were no cCasp3⁺ apoptotic cells in the SVZ or RMS (Fig. 1d). However, 1 week after tamoxifen injection, microglial Mer expression was lost (Extended Data Fig. 5a), and accumulation of apoptotic cells, comparable to that seen in Mertk^{-/-} mice, was detected in the Cx3cr1^{CreER/+}Mertk^{fl/fl} SVZ and RMS (Fig. 1d). Microglia remained

¹Molecular Neurobiology Laboratory, The Salk Institute for Biological Studies, La Jolla, California 92037, USA. ²Instituto de Investigaciones Biomédicas Alberto Sols (CSIC-UAM), Madrid 28029, Spain. ³Waitt Advanced Biophotonics Center, The Salk Institute for Biological Studies, La Jolla, California 92037, USA. ⁴Joint Master in Neuroscience Program, University of Strasbourg, Strasbourg 67081, France. ⁵Department of Immunobiology, Yale University School of Medicine, New Haven, Connecticut 06520, USA. ⁶Immunobiology and Microbial Pathogenesis Laboratory, The Salk Institute for Biological Studies, La Jolla, California 92037, USA.

*These authors contributed equally to this work.

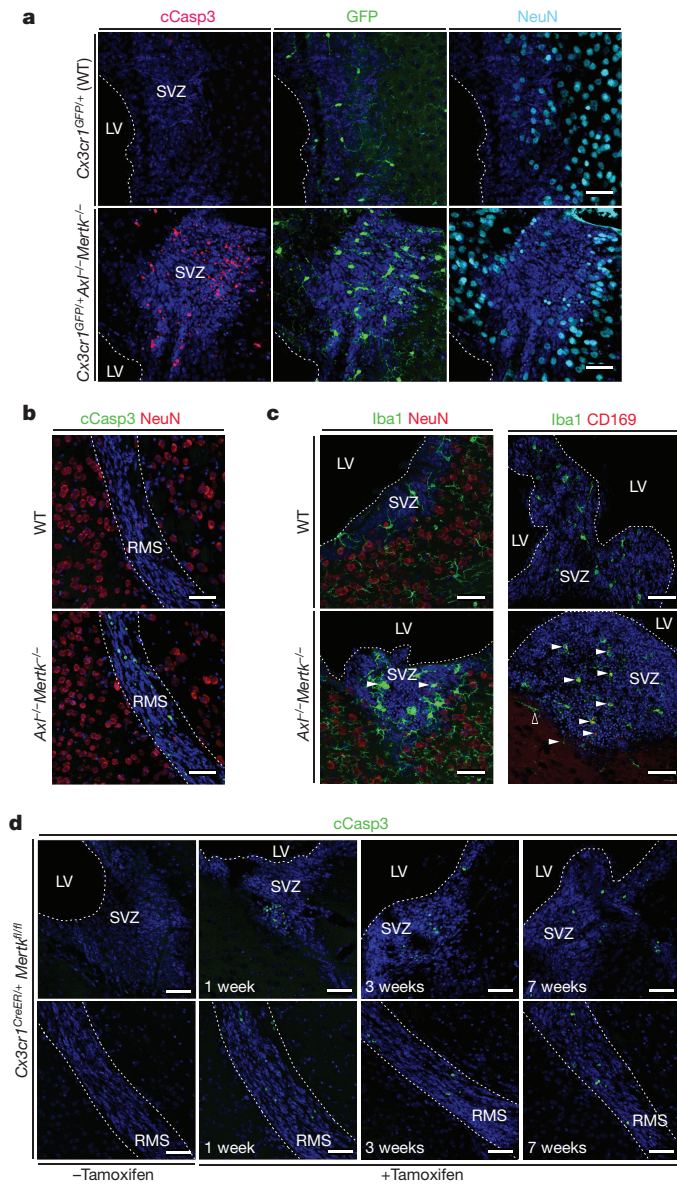


Figure 1 | TAM signalling mediates microglial phagocytosis of apoptotic cells in brain neurogenic regions. **a**, SVZ sections adjacent to the lateral ventricle (LV) of wild-type (WT) or *Axl*^{-/-}*Mertk*^{-/-}*Cx3cr1*^{GFP/+} brains visualized for GFP (green), cCasp3 (magenta), and NeuN (cyan). **b**, RMS of wild-type and *Axl*^{-/-}*Mertk*^{-/-} brains immunostained for cCasp3 (green) and NeuN (red). **c**, Immunostaining of wild-type and *Axl*^{-/-}*Mertk*^{-/-} SVZ with anti-Iba1 (green) and anti-NeuN (red), or anti-Iba1 (green) and anti-CD169 (red). Arrowheads mark Iba1⁺ microglia with an amoeboid morphology (lower left) and Iba1⁺CD169⁺ double-positive microglia (lower right); open arrowhead is an Iba1⁺CD169⁻ cell outside the SVZ. **d**, No cCasp3⁺ apoptotic cells accumulate in the SVZ or RMS of *Cx3cr1*^{CreER/+}*Mertk*^{fl/fl} mice 1 week after vehicle injection (-tamoxifen), but many are evident in the SVZ and RMS at 1, 3, and 7 weeks after injection with vehicle and tamoxifen to induce Cre expression in *Cx3cr1*^{CreER/+} microglia (+tamoxifen). All sections in **a-d** are co-stained with nuclear Hoechst 33258 (blue). Representative images from analyses performed in 3 (**a**, **b**, **d**) and 2 (**c**) mice. Scale bars, 50 μ m.

Mer-negative (Extended Data Fig. 5a) and accumulation of apoptotic cells was maintained at 3 and 7 weeks after tamoxifen injection (Fig. 1d), by which time most *Cx3cr1*^{CreER/+} gene-deleted cells outside the CNS have been replaced by monocytes and/or haematopoietic progenitors²⁴. Mer expression in brain microvascular endothelial cells²³, an important Mer reservoir in the CNS²⁵, persisted following tamoxifen treatment (Extended Data Fig. 5b).

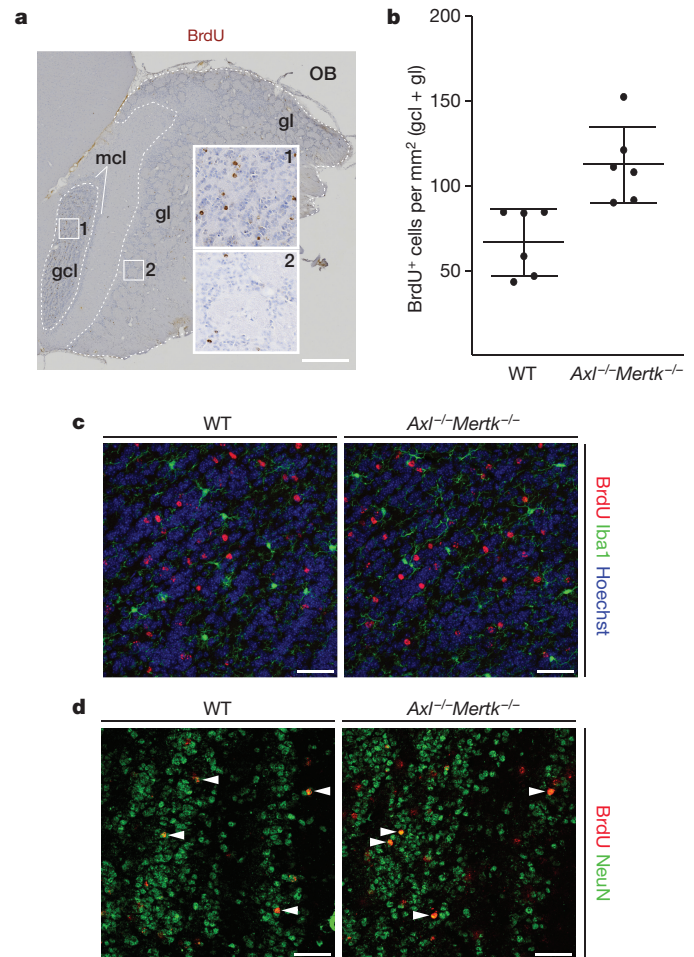


Figure 2 | TAM signalling may mediate death by phagocytosis.

a, *Axl*^{-/-}*Mertk*^{-/-} olfactory bulb section five weeks after BrdU pulse labelling, visualized with an anti-BrdU antibody (brown). The granule cell layer (gcl), glomerular layer (gl), and mitral cell layer (mcl) are indicated, and regions of the granule cell layer (1) and glomerular layer (2) are enlarged. Scale bar, 500 μ m. **b**, Quantification of BrdU⁺ cells per mm² in the granule cell layer and glomerular layer of 6 wild-type versus 6 *Axl*^{-/-}*Mertk*^{-/-} mice. Graph plots average \pm s.e.m.; two-tailed unpaired Mann-Whitney $P = 0.002$. **c**, BrdU⁺ cells in the granule cell layer 35 days after injection of BrdU (red) are negative for Iba1 (green) in wild-type and *Axl*^{-/-}*Mertk*^{-/-} mice. **d**, Similar gcl sections stained with anti-BrdU (red) and NeuN (green). Arrowheads mark NeuN⁺BrdU⁺ cells. Sections in **c** were co-stained with Hoechst 33258. Scale bars (**c**, **d**), 50 μ m. Representative images of $n = 2$ per genotype.

We assessed the consequences of defective clearance of apoptotic cells on neurogenesis by pulse labelling dividing cells in the SVZ of adult mice with bromodeoxyuridine (BrdU), and then counting BrdU⁺ cells that had migrated to the granule cell and glomerular layers of the olfactory bulb 35 days after the pulse (Fig. 2a, b). We found that accumulation of apoptotic cells in the *Axl*^{-/-}*Mertk*^{-/-} SVZ did not reduce the number of BrdU⁺ cells in the olfactory bulb, none of which were apoptotic (Extended Data Fig. 2c) or microglia (Fig. 2c). Indeed, we observed a notable $\sim 70\%$ increase in the number of BrdU⁺ cells in the *Axl*^{-/-}*Mertk*^{-/-} olfactory bulb relative to the wild type (Fig. 2b). This translated to an increased cellular density in the combined granule cell and glomerular layers of the *Axl*^{-/-}*Mertk*^{-/-} olfactory bulb, from 87.7 ± 2.2 nuclei per $10^4 \mu\text{m}^2$ (\pm s.e.m.) in wild type to 99.8 ± 2.4 for the double mutants ($n = 6$ for both genotypes; $P = 0.004$). These results are consistent with the possibility that a fraction of phosphatidylserine (PtdSer)-expressing, but nonetheless viable, SVZ-derived cells are normally 'eaten alive' by microglia, in a process termed 'phagoptosis'²⁶, that this process occurs continuously in a non-pathogenic environment,

and that it is TAM-dependent. Many of the BrdU⁺ cells that had migrated to the *Axl*^{-/-}*Mertk*^{-/-} olfactory bulb were NeuN⁺ (Fig. 2d), and some expressed markers appropriate to their location (Extended Data Fig. 6a, b).

Genetic analyses *in vivo* indicated that both protein S (Pros1) and Gas6 function as Mer agonists for engulfment of apoptotic cells by microglia. The *Gas6*^{-/-} SVZ displayed a wild-type phenotype (Extended Data Fig. 3b), as did the SVZ of *Gas6*^{-/-}*Pros1*^{fl/fl} mice, in which one *Pros1* allele is floxed with loxP sites and the other is inactivated²⁷. (The complete *Pros1*^{-/-} knockout is embryonic lethal²⁷.) In contrast, *Gas6*^{-/-}*Mertk*^{-/-} mice displayed a marked accumulation of cCasp3⁺ cells in the SVZ and RMS, comparable to that seen in *Axl*^{-/-}*Mertk*^{-/-} mice (Extended Data Fig. 3c). We counted $3,638 \pm 282$ (\pm s.e.m.) cCasp3⁺ cells per mm² in the *Gas6*^{-/-}*Mertk*^{-/-} mice SVZ. This is consistent with the fact that Pros1, the only TAM ligand remaining in the *Gas6*^{-/-}*Mertk*^{-/-} mice, does not activate *Axl*⁵, the only microglial TAM receptor remaining in these mice. Thus, as for Mer-dependent phagocytosis in the retina¹⁰, only half of the wild-type level of only a single TAM ligand was sufficient to drive wild-type levels of microglial phagocytosis.

We also quantified phagocytosis of apoptotic cells by microglia cultured from *Cx3cr1*^{GFP/+} mice¹² (Extended Data Fig. 7a). When incubated with apoptotic cells¹² in medium containing 10% serum, where Pros1 is present at ~ 30 nM, wild-type microglia were exceptionally active phagocytes (Extended Data Fig. 7b). Phagocytosis was reduced in *Axl*^{-/-}*Mertk*^{-/-} cells (Extended Data Fig. 7b). In serum-free medium, phagocytosis of apoptotic cells was further reduced, which was mostly TAM-dependent (Extended Data Fig. 7c, d). (This TAM dependence is consistent with the fact that microglia express endogenous *Gas6* and *Pros1* mRNA¹⁷.) When we supplemented serum-free medium with Pros1 or Gas6, we found that both ligands stimulated TAM-dependent phagocytosis (Extended Data Fig. 7c, d). Cultured astrocytes engulfed less apoptotic cells than microglia, and this phagocytosis could be stimulated only modestly by Gas6 (Extended Data Fig. 7e). Stimulation of microglial phagocytosis by both Gas6 and Pros1 demonstrates that it is mediated principally by Mer, as *Axl* is activated only by Gas6^{5,12}.

Although microglia in an uninjured brain are essentially fixed in position, their processes are in constant motion, and survey the entirety of the CNS parenchyma every few hours²⁸. As process extension is also required for phagocytosis¹², we asked if TAM signalling regulates microglial extension velocity. We used *in vivo* two-photon microscopy to measure the movement of microglial processes outside of the neurogenic regions, in the visual cortex of wild-type *Cx3cr1*^{GFP/+} and *Axl*^{-/-}*Mertk*^{-/-}*Cx3cr1*^{GFP/+} mice (Supplementary Videos 2 and 3). Selected video stills, with individual wild-type and *Axl*^{-/-}*Mertk*^{-/-} processes tracked during imaging, are shown in Fig. 3a. These measurements demonstrated that *Axl*^{-/-}*Mertk*^{-/-} microglia, in an uninjured brain, display a $\sim 19\%$ reduction in process extension velocity relative to wild type (Fig. 3b). We also assessed whether TAM signalling was required for microglial responses to injury. We disrupted the blood-brain barrier at the level of individual capillaries with a laser lesion²⁸, and then measured the velocity of microglial process extension towards the lesion site using live two-photon imaging (Supplementary Videos 4 and 5). Selected video stills, with individual extensions towards the lesion tracked in wild-type and *Axl*^{-/-}*Mertk*^{-/-}*Cx3cr1*^{GFP/+} brains, are shown in Fig. 3c. We found that extension towards the laser lesion was $\sim 39\%$ slower in the *Axl*^{-/-}*Mertk*^{-/-} microglia (Fig. 3d). These results demonstrate that routine microglial process activity and the response to injury are both regulated by TAM. They are consistent with the finding that *Mertk*^{-/-} macrophages exhibit compromised cellular migration and a disrupted cytoskeleton *in vitro*²⁹.

For many macrophages, *Axl* and Mer segregate to inflammatory and tolerogenic environments, respectively¹². Inflammatory stimuli such as polyinosinic-polycytidylic acid (poly(I:C)) and interferon γ (IFN γ) upregulate *Axl* expression, whereas immunosuppressive drugs such as

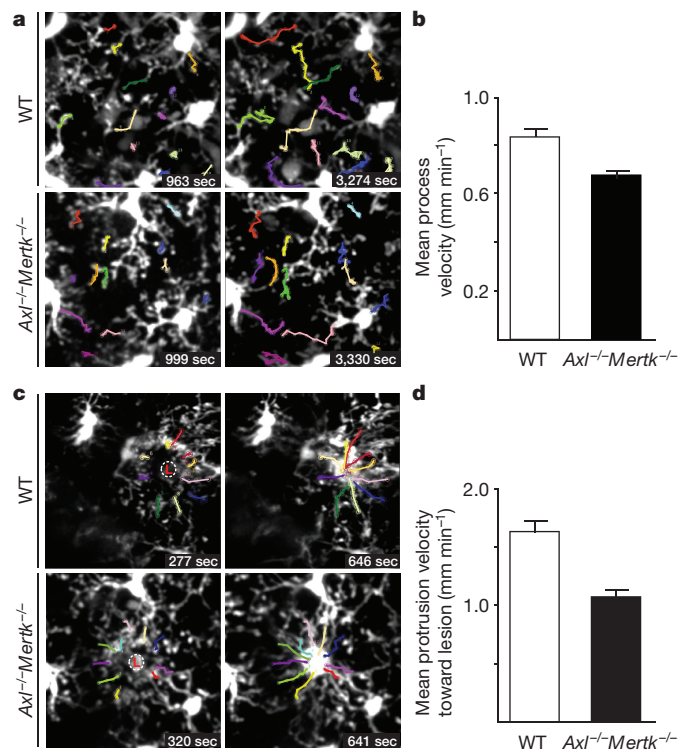


Figure 3 | TAM signalling regulates microglial process extension velocity and response to vascular injury. **a**, Two video stills for wild-type and *Axl*^{-/-}*Mertk*^{-/-} *Cx3cr1*^{GFP/+} mice, with tracking of individual GFP-labelled processes (colour-coded) in the unperturbed visual cortex, by live two-photon imaging. Stills are from Supplementary Videos 2 (wild type) and 3 (*Axl*^{-/-}*Mertk*^{-/-}), and indicated times are from the start of the video. **b**, Mean process velocity (\pm s.e.m.) in the absence of perturbation. $n = 53$ measurements in 3 wild-type mice, and $n = 42$ in 3 *Axl*^{-/-}*Mertk*^{-/-} mice; two-tailed unpaired Mann–Whitney $P = 0.0004$. **c**, Two video stills for wild-type and *Axl*^{-/-}*Mertk*^{-/-} *Cx3cr1*^{GFP/+} mice, illustrating microglial process tracking (colour-coded) towards a laser-induced rupture of a brain microvessel (circled L) by two-photon imaging. Stills are from Supplementary Videos 4 (wild-type) and 5 (*Axl*^{-/-}*Mertk*^{-/-}), and indicated times are from the generation of the laser lesion. **d**, Mean process extension velocity (\pm s.e.m.) towards the lesion site. $n = 20$ measurements in 2 wild-type mice and $n = 30$ in 3 *Axl*^{-/-}*Mertk*^{-/-} mice; two-tailed unpaired Mann–Whitney $P = < 0.0001$.

dexamethasone upregulate Mer¹². We saw similar responses in cultured microglia (Extended Data Fig. 8a, b). As *Axl* is an inflammatory marker, we asked whether its microglial expression might be elevated in neurodegenerative disease¹, and examined a transgenic mouse model of Parkinson's disease. In this model, an alanine 53 to threonine (A53T) mutated form of human α -synuclein (*SNCA*^{A53T}), which leads to a hereditary form of Parkinson's disease, is expressed in neurons, most prominently in the spinal cord, under the control of the mouse *Thy1* promoter⁶. This transgenic expression results in late-onset neurodegeneration, and death at 8–10 months⁶. Measurement of a panel of inflammatory marker mRNAs demonstrated that the spinal cords, and to a lesser extent the brains, of aged *Thy1*-*SNCA*^{A53T} transgenic mice displayed elevation of these markers, whereas inflammation was undetectable in the spleen (Fig. 4a, Extended data Fig. 8c).

The aged transgenic spinal cord, where *SNCA*^{A53T} expression is high (ref. 29 and Fig. 4b), showed markedly elevated expression of Iba1 (Fig. 4b). We also detected upregulation of both *Axl* and soluble *Axl* (s*Axl*) ectodomain, an inflammatory marker¹², in the transgenic cord (Fig. 4c and Extended Data Fig. 8d). In contrast, *Axl* upregulation was undetectable in *Thy1*-*SNCA*^{A53T} spleen and minimal in brain (Extended Data Fig. 8d). No change in Mer expression was detected in the spleen

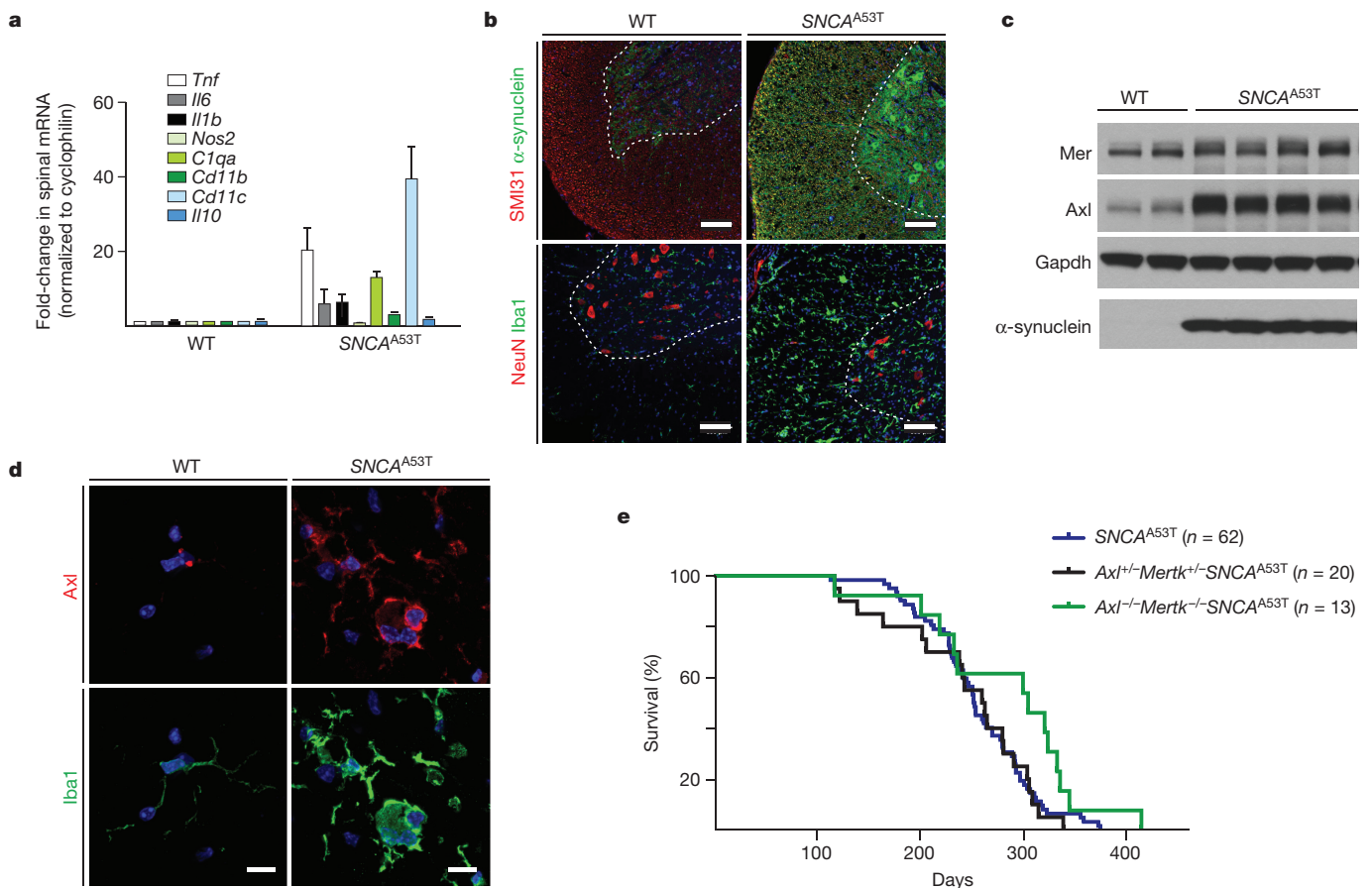


Figure 4 | Microglial Axl is upregulated in a mouse model of Parkinson's disease. **a**, Comparison of the mean expression (\pm s.e.m.) of the indicated inflammatory mediator/marker mRNAs in the spinal cords of 3 wild-type and 3 *Thy1-SNCA^{A53T}* (*SNCA^{A53T}*) mice at 8–10 months of age. **b**, Sections from the spinal cords of aged (8–9 month) wild-type and *SNCA^{A53T}* mice, immunostained for phosphorylated neurofilament (SMI31) and α -synuclein, or NeuN and Iba1. The α -synuclein antibody recognizes both the endogenous mouse protein and the transgenic human protein. Scale bars, 100 μ m. **c**, Western blots of spinal cord extracts from 2 wild-type mice (lanes 1, 2) and 4 *SNCA^{A53T}* mice (lanes 3–6) for the

indicated proteins at 9–10 months of age, with Gapdh as a loading control. **d**, Sections from wild-type and *SNCA^{A53T}* spinal cords immunostained with anti-Axl and anti-Iba1 antibodies. Scale bar, 10 μ m. **e**, Kaplan–Meier survival curves for mice of the indicated genotypes. $n = 62$ *SNCA^{A53T}* mice; 20 *Axl^{+/-}Mertk^{+/-}SNCA^{A53T}*; and 13 *Axl^{-/-}Mertk^{-/-}SNCA^{A53T}* mice. log-rank (Mantel–Cox) test $P = 0.72$ between *SNCA^{A53T}* and *Axl^{+/-}Mertk^{+/-}SNCA^{A53T}*; $P = 0.04$ between *SNCA^{A53T}* and *Axl^{-/-}Mertk^{-/-}SNCA^{A53T}*. Representative images from $n = 2$ wild-type and 3 *SNCA^{A53T}* mice (**b** and **d**).

of the transgenic mice (Extended Data Fig. 8d), with only a very modest increase in the spinal cord (Fig. 4c and Extended Data Fig. 8e). Axl induction in the *Thy1-SNCA^{A53T}* spinal cord was exclusively associated with Iba1⁺ microglia (Fig. 4d). Expression of *SNCA^{A53T}* in spinal motor neurons (ref. 29 and Fig. 4b) leads to progressive ataxia, paralysis, and death, with an onset at ~ 120 days in the transgenic population (Fig. 4e). A 50% reduction in Mer and Axl resulted in no change in this time course, but the loss of both receptors modestly extended survival (Fig. 4e). We do not know the reason for this modest life extension; however, we speculate that wild-type microglia may execute TAM-dependent ‘phagoptotic’ engulfment²⁶ of distressed, PtdSer-displaying motor neurons, thereby speeding up the death of the mice.

Together, the above results identify Mer and Axl as regulators of multiple features of microglial physiology. The elevation in microglial Axl that we document in the *Thy1-SNCA^{A53T}* spinal cord is in keeping with the demonstration that Axl is an inflammatory response receptor in macrophages¹², and that elevated levels of sAxl are observed during multiple human disease and trauma states (ref. 8, and references therein). In this regard, we note that a recent longitudinal study in humans has identified elevated Axl in CSF as among the most reliable indicators of the early appearance of A β pathology and the subsequent development of Alzheimer's disease³⁰.

Online Content Methods, along with any additional Extended Data display items and Source Data, are available in the online version of the paper; references unique to these sections appear only in the online paper.

Received 26 May 2015; accepted 1 March 2016.

Published online 6 April 2016.

- Ransohoff, R. M. & Cardona, A. E. The myeloid cells of the central nervous system parenchyma. *Nature* **468**, 253–262 (2010).
- Lemke, G. Biology of the TAM receptors. *Cold Spring Harb. Perspect. Biol.* **5**, a009076 (2013).
- Aimone, J. B. *et al.* Regulation and function of adult neurogenesis: from genes to cognition. *Physiol. Rev.* **94**, 991–1026 (2014).
- Sierra, A. *et al.* Microglia shape adult hippocampal neurogenesis through apoptosis-coupled phagocytosis. *Cell Stem Cell* **7**, 483–495 (2010).
- Lew, E. D. *et al.* Differential TAM receptor-ligand-phospholipid interactions delimit differential TAM bioactivities. *eLife* **3**, e03385 (2014).
- Chandra, S., Gallardo, G., Fernandez-Chacon, R., Schluter, O. M. & Sudhof, T. C. α -Synuclein cooperates with CSP α in preventing neurodegeneration. *Cell* **123**, 383–396 (2005).
- Ginhoux, F. *et al.* Fate mapping analysis reveals that adult microglia derive from primitive macrophages. *Science* **330**, 841–845 (2010).
- Lu, Q. & Lemke, G. Homeostatic regulation of the immune system by receptor tyrosine kinases of the Tyro 3 family. *Science* **293**, 306–311 (2001).
- Rothlin, C. V., Ghosh, S., Zuniga, E. I., Oldstone, M. B. & Lemke, G. TAM receptors are pleiotropic inhibitors of the innate immune response. *Cell* **131**, 1124–1136 (2007).
- Burstyn-Cohen, T. *et al.* Genetic dissection of TAM receptor-ligand interaction in retinal pigment epithelial cell phagocytosis. *Neuron* **76**, 1123–1132 (2012).

11. Scott, R. S. *et al.* Phagocytosis and clearance of apoptotic cells is mediated by MER. *Nature* **411**, 207–211 (2001).
12. Zagórska, A., Través, P. G., Lew, E. D., Dransfield, I. & Lemke, G. Diversification of TAM receptor tyrosine kinase function. *Nature Immunol.* **15**, 920–928 (2014).
13. Bhattacharyya, S. *et al.* Enveloped viruses disable innate immune responses in dendritic cells by direct activation of TAM receptors. *Cell Host Microbe* **14**, 136–147 (2013).
14. Zhang, Z. *et al.* Activation of the AXL kinase causes resistance to EGFR-targeted therapy in lung cancer. *Nature Genet.* **44**, 852–860 (2012).
15. Lai, C. & Lemke, G. An extended family of protein-tyrosine kinase genes differentially expressed in the vertebrate nervous system. *Neuron* **6**, 691–704 (1991).
16. Prieto, A. L., O'Dell, S., Varnum, B. & Lai, C. Localization and signaling of the receptor protein tyrosine kinase Tyro3 in cortical and hippocampal neurons. *Neuroscience* **150**, 319–334 (2007).
17. Gautier, E. L. *et al.* Gene-expression profiles and transcriptional regulatory pathways that underlie the identity and diversity of mouse tissue macrophages. *Nature Immunol.* **13**, 1118–1128 (2012).
18. Grommes, C. *et al.* Regulation of microglial phagocytosis and inflammatory gene expression by Gas6 acting on the Axl/Mer family of tyrosine kinases. *J. Neuroimmune Pharmacol.* **3**, 130–140 (2008).
19. Ji, R. *et al.* TAM receptors affect adult brain neurogenesis by negative regulation of microglial cell activation. *J. Immunol.* **191**, 6165–6177 (2013).
20. Cardona, A. E. *et al.* Control of microglial neurotoxicity by the fractalkine receptor. *Nature Neurosci.* **9**, 917–924 (2006).
21. Ito, D. *et al.* Microglia-specific localisation of a novel calcium binding protein, Iba1. *Brain Res. Mol. Brain Res.* **57**, 1–9 (1998).
22. Jung, S. *et al.* Analysis of fractalkine receptor CX₃CR1 function by targeted deletion and green fluorescent protein reporter gene insertion. *Mol. Cell. Biol.* **20**, 4106–4114 (2000).
23. Chung, W. S. *et al.* Astrocytes mediate synapse elimination through MEGF10 and MERTK pathways. *Nature* **504**, 394–400 (2013).
24. Parkhurst, C. N. *et al.* Microglia promote learning-dependent synapse formation through brain-derived neurotrophic factor. *Cell* **155**, 1596–1609 (2013).
25. Miner, J. J. *et al.* The TAM receptor MerTK protects against neuroinvasive viral infection by maintaining blood-brain barrier integrity. *Nature Med.* **21**, 1464–1472 (2015).
26. Brown, G. C. & Neher, J. J. Microglial phagocytosis of live neurons. *Nature Rev. Neurosci.* **15**, 209–216 (2014).
27. Burstyn-Cohen, T., Heeb, M. J. & Lemke, G. Lack of protein S in mice causes embryonic lethal coagulopathy and vascular dysgenesis. *J. Clin. Invest.* **119**, 2942–2953 (2009).
28. Nimmerjahn, A., Kirchhoff, F. & Helmchen, F. Resting microglial cells are highly dynamic surveillants of brain parenchyma *in vivo*. *Science* **308**, 1314–1318 (2005).
29. Tang, Y. *et al.* MerTK deficiency affects macrophage directional migration via disruption of cytoskeletal organization. *PLoS ONE* **10**, e0117787 (2015).
30. Mattsson, N. *et al.* CSF protein biomarkers predicting longitudinal reduction of CSF β -amyloid42 in cognitively healthy elders. *Transl. Psychiatry* **3**, e293 (2013).

Supplementary Information is available in the online version of the paper.

Acknowledgements This work was supported by grants from the US National Institutes of Health (R01 NS085296 and R01 AI101400 to G.L., DP2 NS083038 and R01 NS085938 to A.N., R01 AI089824 to C.V.R., and P30CA014195 to the Salk Institute), the Leona M. and Harry B. Helmsley Charitable Trust (#2012-PG-MED002 to the Salk Institute), the Nomis, H. N. and Frances C. Berger, Fritz B. Burns, and HKT Foundations (to G.L.), and the Waitt, Rita Allen and Hearst Foundations (to A.N.); and by postdoctoral fellowships from the Marie Curie International Outgoing Fellowship Program (to P.G.T.), the Nomis Foundation (to A.Z. and E.D.L.), and the Howard Hughes Medical Institute Life Sciences Research Foundation (to Y.T.). We thank J. Hash for excellent technical assistance and J. Flynn for help with the CLARITY method.

Author Contributions L.F. and P.G.T. designed experiments, performed apoptotic cell, BrdU, immunohistochemical, and genetic analyses, and contributed equally to the paper; Y.T., L.F. and H.L.-B. performed and analysed *in vivo* two photon imaging; E.D.L. prepared TAM ligands; P.G.B. performed brain histology; P.C. analysed cytokine profiles; A.Z. analysed Axl expression in Parkinson's disease transgenics; C.V.R. provided floxed *Mertk* alleles; A.N. designed and implemented two-photon imaging; and G.L. designed experiments and wrote the paper. All authors edited the paper.

Author Information Reprints and permissions information is available at www.nature.com/reprints. The authors declare no competing financial interests. Readers are welcome to comment on the online version of the paper. Correspondence and requests for materials should be addressed to G.L. (lemke@salk.edu) or C.V.R. (carla.rothlin@yale.edu); for requests for floxed *Mertk* alleles).

METHODS

Mice. The *Axl*^{-/-31}, *Merk*^{-/-31}, *Axl*^{-/-}*Merk*^{-/-31}, *Gas6*^{-/-31}*Prosl*^{fl/fl}*NesCre*^{10,32}, *Prosl*^{fl/fl}*NesCre*¹⁰, *Cx3cr1*^{GFP/+22}, *Cx3cr1*^{CreER24}, *S100b*^{GFP/+33} and *SNCA*^{A53T} (ref. 6) strains have been described previously. The *Merk*^{fl/fl} mouse line diagrammed in Extended Data Fig. 4 was generated by inGenious Targeting Laboratory (iTLL, Ronkonkoma NY), using iTLL C57Bl/6 embryonic stem (ES) cells. This line targets exon 18, a 137 nucleotide (nt) sequence that encodes residues W779–L824 within the Mer kinase domain. Cre-mediated deletion of this exon introduces a frame shift and a stop codon one amino acid downstream of exon 17. This truncated, kinase-dead protein and/or its mRNA are apparently unstable, as antibodies directed against the Mer extracellular domain do not detect a truncated protein upon Cre-mediated excision (see text). Deletion of exon 18 therefore effectively generates a protein null. The complete *Merk* mouse knockout³¹ deletes exon 17, a 160 nt sequence that encodes M725–V778 within the Mer kinase domain. (Exon 17 was numbered as exon 18 in the original description of the *Merk* knockout allele³¹.) This single exon deletion also introduces a frame shift (five amino acids downstream of exon 16), produces an unstable protein, and also results in a Mer protein null¹². The Neo cassette was removed via FLP-mediated recombination by crossing high-percentage chimaeric mice to C57Bl/6 FLP mice. Neo deletion was confirmed by PCR. These *Merk*^{fl/fl} mice, together with PCR-based protocols for their genotyping, are available upon request from the Rothlin laboratory (contact C.V.R.). Recombination (inactivation) of the *Merk*^{fl/fl} allele in *Cx3cr1*^{CreER/+}*Merk*^{fl/fl} mice was achieved using tamoxifen injection. *Cx3cr1*^{CreER/+}*Merk*^{fl/fl} mice (16 weeks) received a dose (150 mg kg⁻¹ body weight) of tamoxifen (Sigma) as a solution in corn oil (Sigma) by intraperitoneal (i.p.) injection. Control mice received an i.p. injection of vehicle (corn oil) alone. Mice were analysed for Mer expression and apoptotic-cell (cCasp3⁺ cell) accumulation 1 week, 3 weeks or 7 weeks after injection. Mice analysed at 1 week received a single dose of tamoxifen or oil; mice analysed at 3 and 7 weeks received two successive injections 48 h apart. All lines, with the exception of the *Merk*^{fl/fl} alleles, have been backcrossed for >9 generations to a C57Bl/6 background. All animal procedures were conducted according to protocols approved by the Salk Institute Animal Care and Use Committee (Protocol No. 11-00051). Mice (both males and females) were randomly allocated to experimental groups (three to six mice per group) and investigators were blinded to group allocation during the experiment. Investigators were not blinded to sample identity. Group size was based on previous literature. No statistical methods were used to predetermine sample size.

Reagents and antibodies. Dexamethasone, 5-Bromo-2-deoxyuridine and DMSO were from Sigma-Aldrich. Poly(I:C) was from Invivogen. Lipopolysaccharide (LPS) (*Escherichia coli* serotype O55:B5) was from Enzo. IFN- γ was from BioVision. Purified human protein S was from Haematologic Technologies. Recombinant mouse Gas6 was produced as described previously⁵. Antibodies used were as follows: anti-Mer (AF591), anti-Axl (AF854), and anti-Gas6 (AF986) were from R&D Systems, anti-Mer (DS5MMER) from eBioscience, anti-Iba1 (019-19741) was from Wako, anti-GFAP (z0334) was from Dako, anti-Neurofilament H (SMI-31 NE1022), anti-NeuN (MAB377 A60), anti-Calretinin (AB1550), anti-Tyrosine Hydroxylase (MAB318; LNC1) and anti-GAPDH (MAB374; 6C5) were from Millipore, anti- α -synuclein (C-20-R sc-7011-R) and anti-Axl (M-20 sc-1097) were from Santa Cruz, anti-cCaspase 3 (Asp175) was from Cell Signaling, anti-ACSA-2 (clone IH3-18A3) was from Miltenyi Biotec, anti-CD169 (Siglec1; 3D6) and anti-BrdU (BU1/75 (ICR1) were from AbD serotec, and anti CD31 (ab28364) and anti-S100b (EP1576Y) were from Abcam. Secondary antibodies used for immunoblot analysis were horseradish-peroxidase-conjugated anti-goat (705-035-003) from Jackson ImmunoResearch, and anti-mouse (NA931V) and anti-rabbit (NA934V) from GE Healthcare. Secondary antibodies for immunocyto- and immunohistochemistry were fluorophore-conjugated anti-goat (A-11055 from Life Technologies, or 705-166-147 from Jackson ImmunoResearch), anti-rabbit (A-10040 or A-21206 from Life Technologies), and anti-mouse (A-11029 from Life Technologies, or 715-166-150 from Jackson ImmunoResearch).

Immunohistochemistry. Adult mice (3–6 month) were anaesthetized with 2.5% avertin in saline, perfused with 20 U ml⁻¹ heparin in PBS, and subsequently with 4% PFA in PBS. Brain and spinal cords were collected, immersion-fixed overnight at 4°C, infiltrated with 30% sucrose in PBS overnight at 4°C, and flash-frozen in tissue freezing medium. Sections of 17 μ m were cut, air-dried overnight at room temperature and subsequently processed for staining. Non-specific binding was blocked by 1 h incubation in blocking buffer (PBS containing 0.1% Tween-20, 5% donkey serum and 2% IgG-free BSA). Sections were incubated overnight at 4°C with primary antibody (identified above) diluted in blocking buffer, then washed in PBS 0.1% Tween-20, and incubated for 2 h at 22–24°C in the dark with Hoechst and fluorophore-coupled secondary antibodies diluted in blocking buffer. Sections were washed, sealed with Fluoromount-G (SouthernBiotech) and stored at 4°C. Images were acquired with a Zeiss LSM 710 confocal microscope using Plan-Apochromat 40 \times and 63 \times objectives.

Quantification of apoptotic cells. Cleaved Casp3⁺ apoptotic cells were counted in four successive 17 μ m sections that spanned the SVZ in three different mice for both the *Merk*^{-/-} and *Axl*^{-/-}*Merk*^{-/-} genotypes, and in two different mice for the *Merk*^{-/-}*Gas6*^{-/-} genotype. No cCasp3⁺ cells in excess of wild-type were observed in SVZ sections of any of the other genotypes analysed. The cross-sectional area of the SVZ was defined as the region of intense Hoechst 33258 staining, as illustrated in Figs 1a, c, d, and measured using ImageJ. Accumulation of apoptotic cells between the *Axl*^{-/-}*Merk*^{-/-} and *Merk*^{-/-}*Gas6*^{-/-} genotypes is not statistically different. Note that cCasp3 marks a subset of apoptotic cells.

BrdU pulse labelling. Three successive injections (50 mg kg⁻¹ body weight) of 5-bromo-2-deoxyuridine (BrdU) were performed in 8-week-old mice at 24 h intervals and BrdU staining was assessed 35 days later. Briefly, mice were anaesthetized with 2.5% avertin in saline, perfused with 20 U ml⁻¹ heparin in PBS, and subsequently with 4% PFA in PBS. Brain were collected, immersion fixed overnight at 4°C, infiltrated with 30% sucrose in PBS overnight at 4°C and flash-frozen in tissue freezing medium. Sections of 17 μ m were cut and air-dried overnight at room temperature. Subsequently, the sections were incubated in 2 N HCl at 37°C for 30 min, rinsed for 10 min in 0.1 M borate buffer (pH 8.4) at room temperature and washed six times in PBS. To block endogenous peroxidase activity, sections were incubated for 10 min in 0.3% H₂O₂ in 10% methanol. Non-specific binding was blocked by 1 h incubation in blocking buffer (PBS containing 0.25% Triton-X and 5% donkey serum). Sections were incubated for 72 h at 4°C with primary antibody (anti-BrdU) diluted in blocking buffer, then washed in PBS 0.1% Tween-20, and incubated for 2 h at room temperature in the dark with a biotin-conjugated secondary antibody diluted in blocking buffer. Sections were washed and 3,3'-diaminobenzidine (DAB) staining was performed using Vectastain Elite ABC-kit (Vector Laboratories) and DAB peroxidase (HRP) substrate kit (Vector Laboratories) following manufacturer's instructions. Afterwards, sections were counterstained using haematoxylin for 15 s, sealed with Vectamount (Vector Laboratories) and stored at room temperature. Images were acquired with a Zeiss slide scanner Axio Scan.Z1 using 20 \times objective and analysed with ImageJ. For quantitation, BrdU⁺ cells in granule cell layer and glomerular layer of the olfactory bulb were counted in two consecutive sections per animal and averaged per animal.

Immunocytochemistry. Cells were fixed for 10 min in 4% PFA/4% sucrose in PBS, washed with PBS, incubated for 10 min in 100 mM glycine, permeabilized for 5 min in 0.2% Triton-X100 in PBS, washed with PBS, and nonspecific binding was then blocked by 40 min incubation in blocking buffer (2% IgG-free BSA in PBS). Coverslips were incubated for 1 h at 22–24°C with primary antibody diluted in blocking buffer, washed five times in PBS, and then incubated for 1 h at 22–24°C in the dark with Hoechst stain and fluorophore-coupled donkey secondary antibody (identified above) diluted in blocking buffer. Coverslips were washed and mounted on slides with Fluoromount-G (SouthernBiotech) and stored at 4°C. Images were acquired with a Zeiss LSM 710 confocal microscope using Plan-Apochromat 40 \times and 63 \times objectives.

CLARITY imaging. One cerebral hemisphere from a *Cx3cr1*^{GFP/+} mouse was cleared using CLARITY protocols, essentially as described³⁴. Rather than electrophoretic clearing, samples were incubated at 37°C and passively cleared over 3 weeks by daily replacement of the clearing solution. A 1 mm³ block of tissue adjacent to the lateral ventricle of *Cx3cr1*^{GFP/+} mice, in the region containing the SVZ, was imaged using a Zeiss LSM 710 confocal microscope. Fiji software was used to assemble images.

Immunoblot. Cultured cells were washed with ice-cold DPBS and lysed on ice in 50 mM Tris-HCl (pH 7.5), 1 mM EGTA, 1 mM EDTA, 1% Triton-X100, 0.27 M sucrose, and protease and phosphatase inhibitors (Roche). Tissues were snap-frozen in liquid nitrogen before lysis. For immunoblot analysis, equal amounts of protein in LDS sample buffer (Invitrogen) were separated by electrophoresis through 4–12% Bis-Tris polyacrylamide gels (Novex, Life Technologies) and transferred to PVDF membranes (Millipore). For Axl immunoprecipitation, tissue lysates were precleared overnight at 4°C with Protein G-Sepharose (Invitrogen). This was then removed and lysates were incubated for 2 h with 0.2 μ g anti-Axl (M20) for 0.5 mg protein in cell lysate. Fresh Protein G-Sepharose was added for 2 h and immunoprecipitates were washed twice with 1 ml of lysis buffer containing 0.5 M NaCl and once with 1 ml of 50 mM Tris-HCl (pH 7.5). Immunoprecipitates were eluted in LDS buffer, separated by electrophoresis through polyacrylamide gels and transferred to PVDF membranes. Nonspecific binding was blocked with TBST (50 mM Tris-HCl (pH 7.5), 0.15 M NaCl and 0.1% Tween-20) containing 5% BSA, and membranes were incubated overnight at 4°C with primary antibodies diluted in blocking buffer. Blots were then washed in TBST and incubated for 1 h at 22–24°C with secondary horseradish peroxidase-conjugated antibodies in 5% skim milk in TBST. After repeating the washes, signal was detected with enhanced chemiluminescence reagent.

Reverse transcription (RT)-qPCR. Total cellular RNA was isolated with an RNeasy Mini Kit according to the manufacturer's instructions (Qiagen).

DNA was removed by on-column digestion with DNase (Qiagen). An RT Transcriptor First Strand cDNA Synthesis Kit (Roche) with anchored oligonucleotide (dT) primers (Roche) was used for reverse transcription. Quantitative PCR was run in a 384-well plate format on a ViiA 7 Real-Time PCR System (Applied Biosystems) with 2 × SYBR Green PCR Master Mix (Applied Biosystems). Primers are listed in Supplementary Table 1. Expression was analysed by the threshold cycle ($\Delta\Delta C_T$).

Microglia and astrocyte culture. Postnatal day 30 (P30) to P50 mice (*Cx3cr1^{GFP/+}*, *Axl^{-/-}Mertk^{-/-}Cx3cr1^{GFP/+}*) brains were dissociated using Neural Dissociation kit, Postnatal Neurons and the gentleMACS dissociator according to the manufacturer's instructions (Miltenyi). Single cell suspensions were resuspended in 30% Percoll in HBSS solution and centrifuged 15 min at 700 g to remove myelin. Cells were grown for 7 days in DMEM-F12 with 10% fetal bovine serum (FBS) and 1% penicillin/streptomycin before being processed for immunostaining or phagocytosis assay. Cytosine β -D-arabino-furanoside (Ara-C, 5 μ M) was added after 5 days *in vitro* to limit fibroblast proliferation. When astrocytes were also isolated, microglia were first purified using C11b MicroBeads (Miltenyi) and grown for 7 days in DMEM-F12 with 10% FBS and 1% penicillin/streptomycin while astrocytes were grown for 10 days in MACS Neuro Medium with 2% MACS NeuroBrew-21 and 1% penicillin/streptomycin.

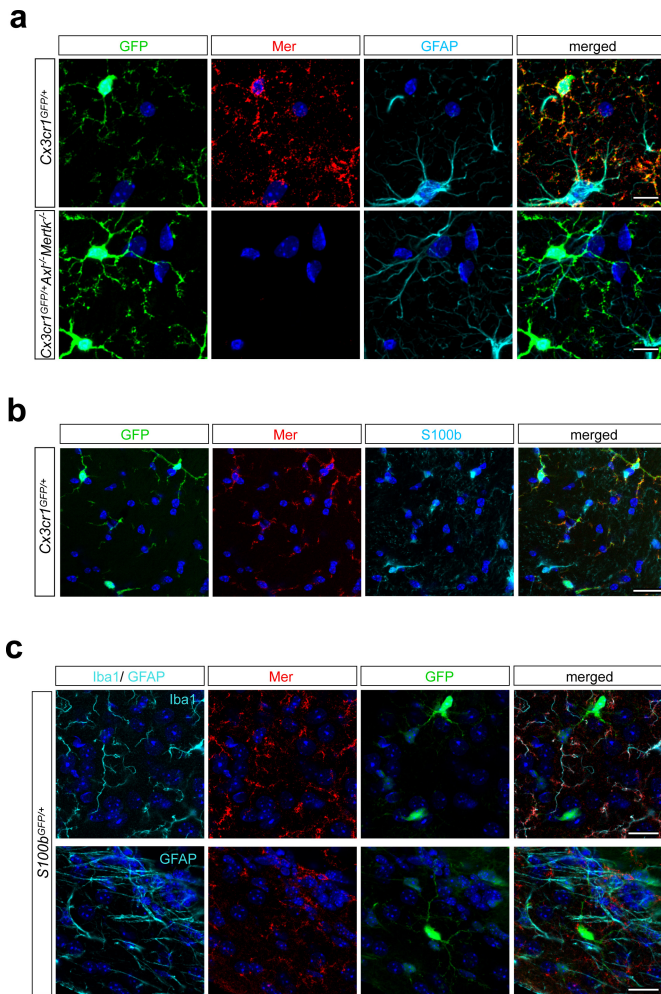
Phagocytosis assay. For the generation of apoptotic cells, thymocytes were isolated from 3- to 6-week-old mice, red blood cells were lysed with ACK buffer and remaining cells were incubated for 6 h in RPMI medium containing 5% FBS and 2 μ M dexamethasone to induce apoptosis. This routinely resulted in 70% apoptotic and \leq 5% necrotic cells. Apoptotic cells were then stained for 30 min with 100 ng ml⁻¹ pHrodo-s.e. (Invitrogen) as described previously^{12,35,36}. Labelled cells were washed twice in PBS containing 1% BSA (to block remaining pHrodo-SE) and 1 mM EDTA (to remove any bound Gas6 and protein S) and once with DMEM. Apoptotic cells were then incubated for 10 min with recombinant mouse Gas6 or purified human protein S, added to microglia or astrocyte cultures at a ratio of 10:1 (apoptotic cells:phagocytes), and incubated for 1 h at 37 °C. Microglia or astrocytes were then briefly washed in DPBS, incubated for 10 min at 37 °C in trypsin (0.25%), and then placed on ice and detached by vigorous pipetting. Astrocytes were labelled using anti-ACSA2-APC antibody³⁷. Phagocytosis was assessed by flow cytometry with post-acquisition data analysis with FlowJo software (TreeStar). pHrodo fluorescence was measured with excitation at 561 nm and emission filters for phycoerythrin (574–590 nm) on a LSR II (BD Biosciences) at the Flow Cytometry Core of the Salk Institute, as described previously¹². Microglia were gated as GFP⁺ cells and astrocytes were gated as APC⁺ cells.

Two-photon imaging. Adult male mice (3–6 months old) were anaesthetized with isoflurane (1.5–2.5% in 100% oxygen at 0.8–1.0 l min⁻¹). Body temperature was kept at 36–37 °C, and hydration status was maintained using subcutaneous physiological saline injections (0.1 ml per 25 g body weight every 1–2 h). For head plate implantation, hair, skin and periosteum overlying the neocortex were removed. After cleaning exposed skull areas, a custom metal head plate was affixed to the skull using OptiBond (31514; Kerr) and dental acrylic (H00335; Coltene Whaledent), keeping the intended imaging area over somatosensory or visual cortex uncovered. A polished and reinforced thinned skull window (\sim 2–3-mm diameter; \sim 20–50 μ m remaining bone thickness) was then prepared, as described previously^{38,39}. A movable objective microscope (Sutter Instrument) equipped with a pulsed femtosecond Ti:Sapphire laser (Chameleon Vision II or Ultra II, Coherent), two fluorescence detection channels (565DXCR

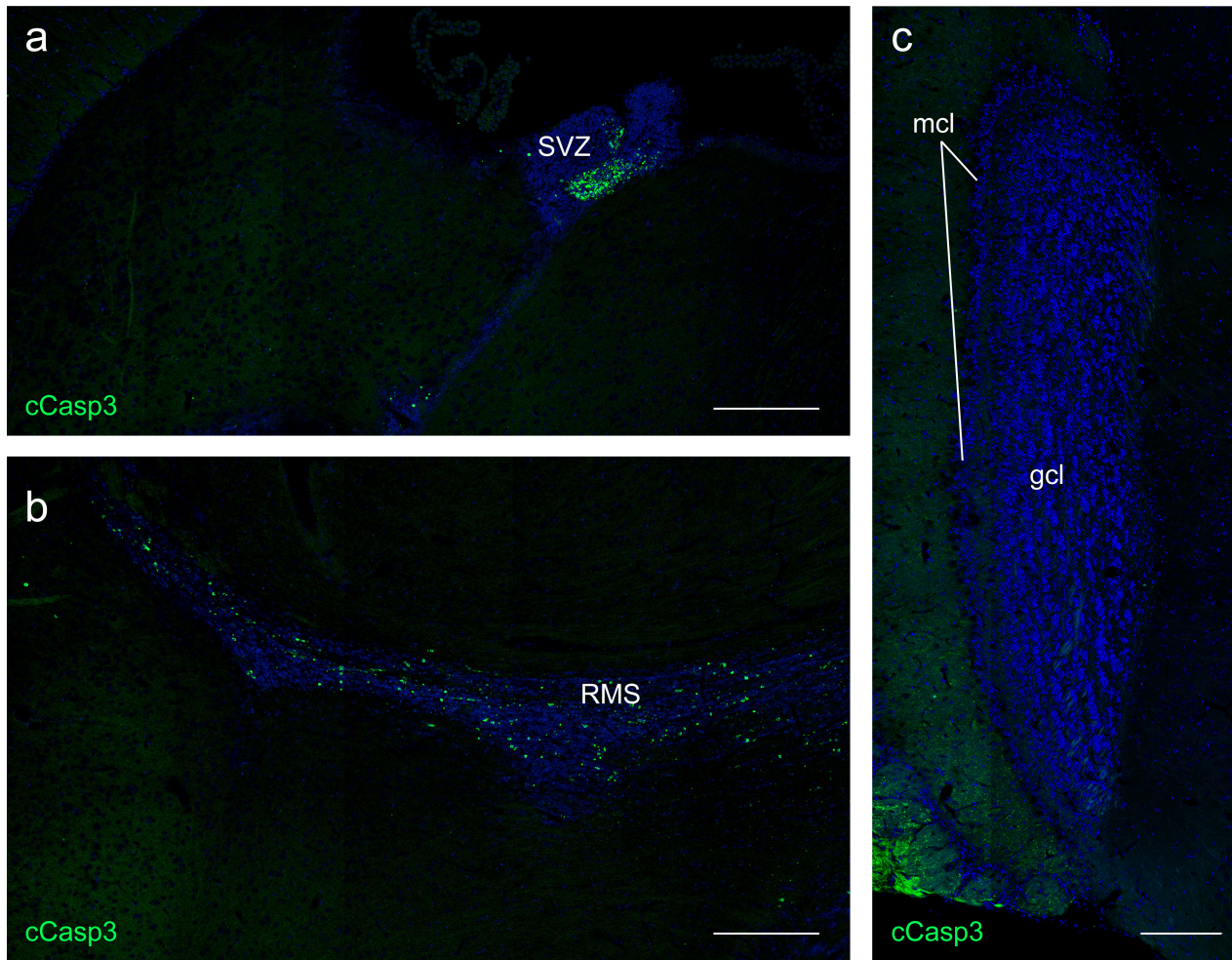
dichroic, ET525/70M-2P and ET605/70M-2P emission filters, Chroma; H7422-40 GaAsP photomultiplier tubes, Hamamatsu), and a water immersion objective (LUMPlanFL N 40XW 0.8NA; Olympus) was used for two-photon imaging. Imaging was performed as described previously^{28,39} using 920–940 nm centre excitation wavelengths. Average laser powers used for transcranial optical recordings depended on imaging depth (typically \sim 10–30 mW at \sim 150–200 μ m depth from the pia). Images were typically acquired using a 6 Hz frame rate, 256 × 256 pixel resolution and a 5-frame average. Image stacks were acquired every 1.5–2 min for up to 5 h and typically contained 20–30 images per stack with 1 μ m axial image spacing. Fields-of-view had a typical side length of 65–100 μ m. Imaging settings were kept constant during time-lapse recordings. For quantitative image data analysis, ImageJ or Fiji software was used. First, maximum intensity images were produced from individual image stacks. Then, lateral image shifts in time-lapse recordings were corrected using a custom-written ImageJ alignment plugin based on the position shift of the peak in cross-correlation images, typically using the first projection image as the reference image. Structural dynamics of individual microglial cell processes was quantified manually using the MTrackJ plugin in Fiji. Image analysis was done blind with respect to experimental condition. Videos were also created with Fiji.

Laser lesion. To target blood vessels for focal laser lesion, blood plasma was stained by tail vein injection of biocytin-TMR (2–5% in saline, T-12921, Life Technologies). Lesions were performed following a baseline recording period of 30–45 min, during which z-stacks were acquired as described above. To induce lesions, the Ti:Sapphire laser was transiently tuned to 800 nm and a confined area (8–15 μ m diameter, \sim 1 μ m axial extent) of a horizontally oriented cortical capillary at 150–220 μ m depth was exposed to 70–130 mW for 10–30 s. Laser lesions caused extravasation of dye, indicating disruption of the blood-brain barrier. Following focal lesion, image stack acquisition was resumed using the same laser and recording parameters as during the baseline recording period. Although Supplementary Videos 4 and 5 run for only \sim 12 min (the time required for microglial processes to reach the lesion site), time-lapse recording of the same cortical volume continued for 2–4 h after the lesion.

- Lu, Q. *et al.* Tyro-3 family receptors are essential regulators of mammalian spermatogenesis. *Nature* **398**, 723–728 (1999).
- Angelillo-Scherrer, A. *et al.* Deficiency or inhibition of Gas6 causes platelet dysfunction and protects mice against thrombosis. *Nature Med.* **7**, 215–221 (2001).
- Vives, V., Alonso, G., Solal, A. C., Joubert, D. & Legraverend, C. Visualization of S100B-positive neurons and glia in the central nervous system of EGFP transgenic mice. *J. Comp. Neurol.* **457**, 404–419 (2003).
- Chung, K. *et al.* Structural and molecular interrogation of intact biological systems. *Nature* **497**, 332–337 (2013).
- Miksa, M., Komura, H., Wu, R., Shah, K. G. & Wang, P. A novel method to determine the engulfment of apoptotic cells by macrophages using pHrodo succinimidyl ester. *J. Immunol. Methods* **342**, 71–77 (2009).
- Dransfield, I., Zagorska, A., Lew, E. D., Michail, K. & Lemke, G. Mer receptor tyrosine kinase mediates both tethering and phagocytosis of apoptotic cells. *Cell Death Dis.* **6**, e1646 (2015).
- Sharma, K. *et al.* Cell type- and brain region-resolved mouse brain proteome. *Nature Neurosci.* **18**, 1819–1831 (2015).
- Drew, P. J. *et al.* Chronic optical access through a polished and reinforced thinned skull. *Nature Methods* **7**, 981–984 (2010).
- Knowland, D. *et al.* Stepwise recruitment of transcellular and paracellular pathways underlies blood-brain barrier breakdown in stroke. *Neuron* **82**, 603–617 (2014).

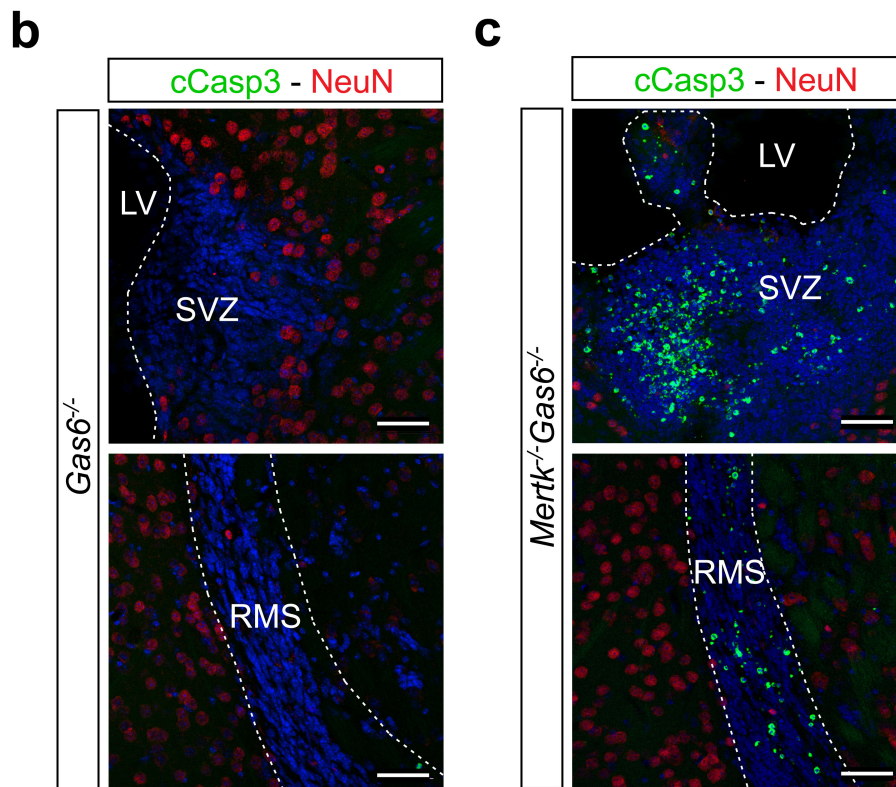
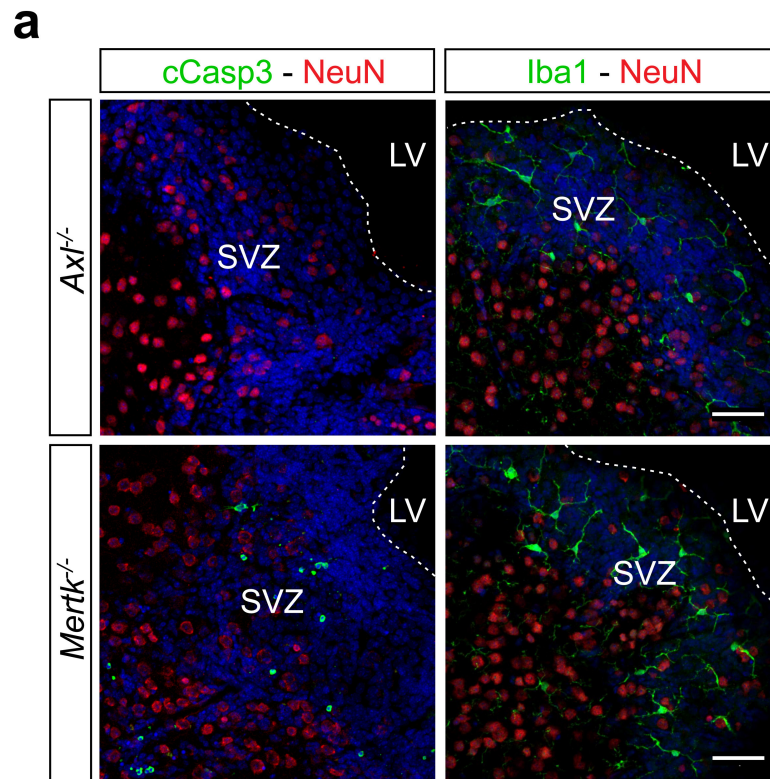


Extended Data Figure 1 | Mer is expressed by microglia. **a**, Brain (hippocampus) sections from *Cx3cr1^{GFP/+}* mice that were wild-type (top row) or *Axl^{-/-}Mertk^{-/-}* (bottom row) were visualized by confocal microscopy for GFP (1st column), anti-Mer (red, 2nd column), or anti-GFAP (cyan, 3rd column) immunoreactivity; 4th column, merged images. Scale bars, 10 μ m. Axl immunostaining signal is too low to be visualized in unactivated microglia (not shown; but see Fig. 4d). **b**, Mer expression does not co-localize with S100b⁺ cells. Immunostaining of *Cx3cr1^{GFP/+}* brain sections with anti-Mer (red, 2nd panel) and anti-S100b (cyan, 3rd panel); 4th panel, merged images. **c**, Mer co-localizes with Iba1, but not GFAP or GFP in *S100b^{GFP/+}* mice. Brain sections were visualized by confocal microscopy for anti-Iba1 (top) or anti-Gfap (bottom) (both cyan, 1st column), anti-Mer (red, 2nd column), or GFP (green, 3rd column) immunoreactivity; 4th column, merged images. Scale bars (**b**, **c**), 20 μ m. Representative images from analyses performed in $n = 2$ mice (**a-c**).



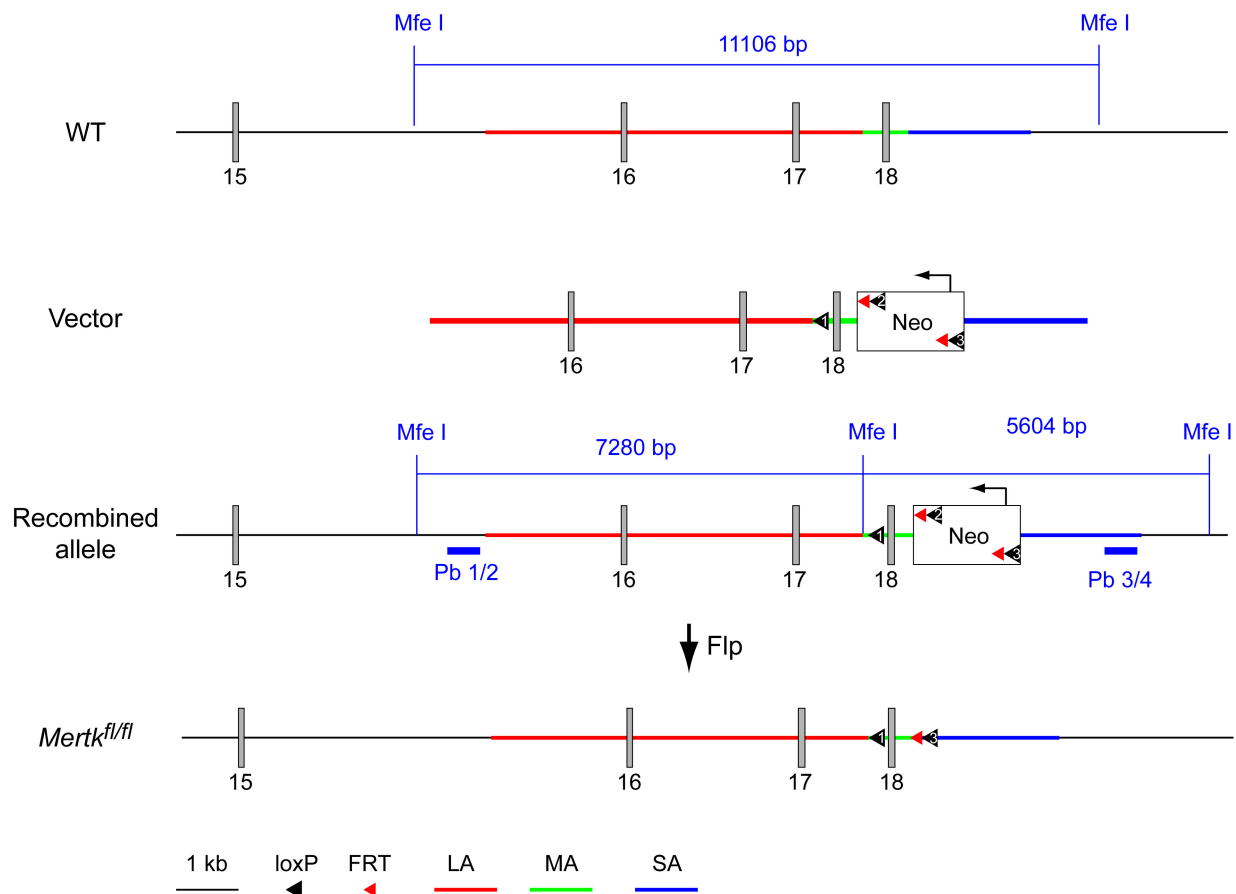
Extended Data Figure 2 | Accumulation of apoptotic cells is confined to neurogenic and derivative migratory regions of the $Axl^{-/-}Mertk^{-/-}$ CNS. **a**, A low power tiled image of a section through the $Axl^{-/-}Mertk^{-/-}$ subventricular zone and surrounding brain tissue, stained for cCasp3, illustrates that apoptotic cells are confined within the SVZ. **b**, A low power tiled image of a section through the $Axl^{-/-}Mertk^{-/-}$ rostral migratory stream (RMS) and surrounding brain tissue illustrates that cCasp3⁺

apoptotic cells are confined within the RMS. **c**, A low power tiled image of the granule cell and mitral cell layers (gcl and mcl, respectively) of the $Axl^{-/-}Mertk^{-/-}$ olfactory bulb, stained for cCasp3, illustrates that there are no apoptotic cells detected in the double mutant bulb. Scale bars (a–c), 200 μ m. Representative images from analyses performed in $n = 3$ mice (a–c).



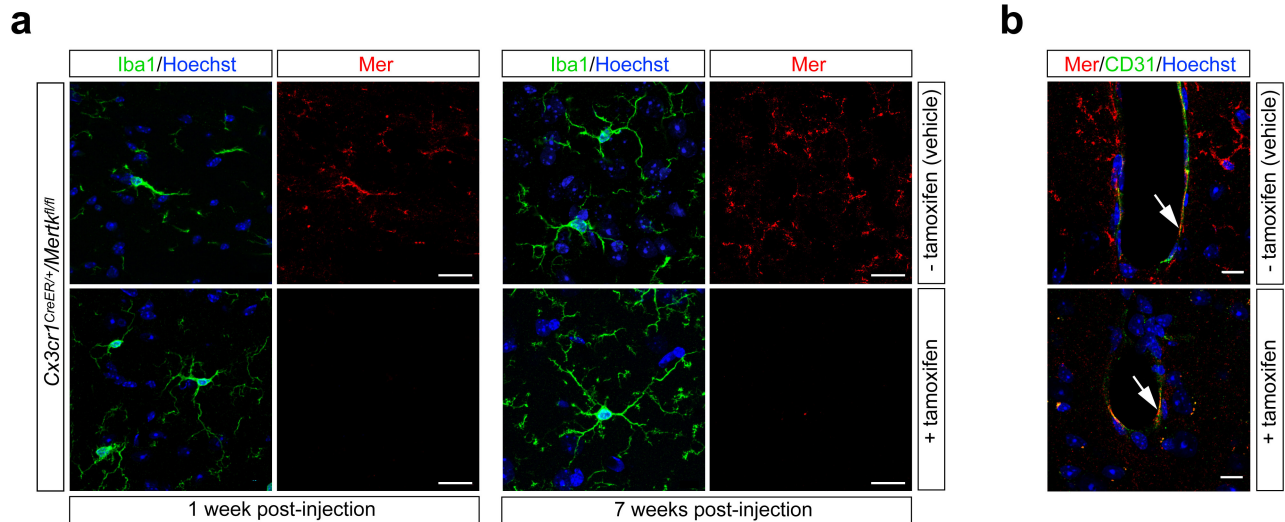
Extended Data Figure 3 | Mer is the principal microglial TAM receptor required for phagocytosis of apoptotic cells in the SVZ. **a**, Sections of the SVZ from *Axl*^{-/-} (top row) and *Mertk*^{-/-} (bottom row) mice immunostained for cCasp3 and NeuN (green and red, respectively; left panels), or Iba1 and NeuN (green and red, respectively; right panels) reveal the accumulation of cCasp3⁺ apoptotic cells only in the *Mertk*^{-/-} SVZ. **b**, Sections of the SVZ (top) and RMS (bottom) of *Gas6*^{-/-} mice,

illustrating no accumulation of apoptotic cells (similar to both wild type and *Axl*^{-/-}). **c**, Sections of the SVZ (top) and RMS (bottom) of *Mertk*^{-/-}*Gas6*^{-/-} mice, illustrating a massive accumulation of apoptotic cells, similar to that seen in *Axl*^{-/-}*Mertk*^{-/-} mice. Scale bars, 50 μ m. See main text for quantification. Representative images from analyses performed in $n = 2$ mice for *Gas6*^{-/-} and *Mertk*^{-/-}*Gas6*^{-/-}, and $n = 3$ mice for *Axl*^{-/-} and *Mertk*^{-/-}.



Extended Data Figure 4 | Conditional *Mertk* knockouts. The knockout strategy targets exon 18 of the wild-type mouse *Mertk* gene, which encodes residues W779–L824 of the tyrosine kinase domain (1st line). Deletion of this exon leads to a functional and null protein (see Methods, and Extended Data Fig. 5). The targeting vector (2nd line) had a PGK-Neo cassette for selection in embryonic stem (ES) cells, and contained loxP and FRT sites, recognized by Cre and Flp recombinases, respectively, at the indicated positions. Five ES cell lines with homologous recombination at the *Mertk* locus were identified by Southern blots of MfeI-digested

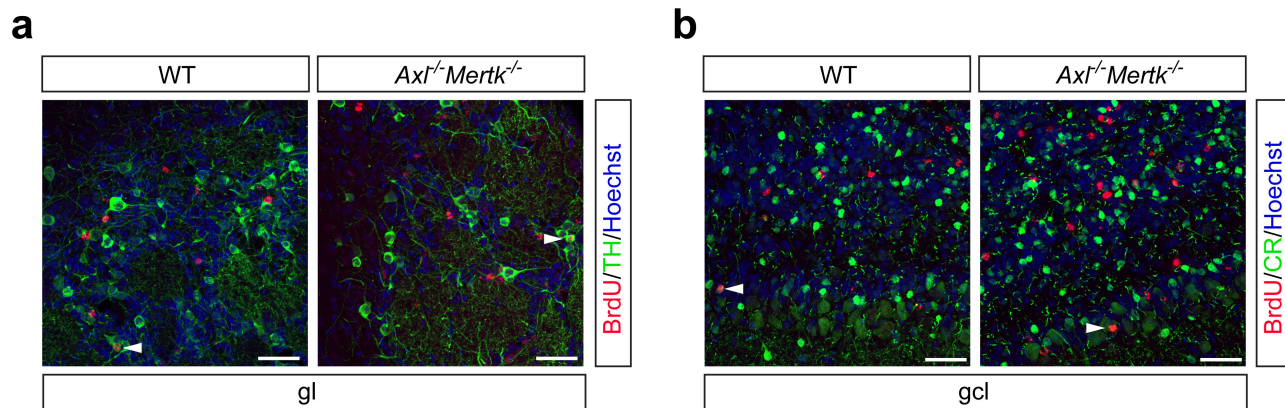
DNA, using the indicated Pb 1/2 (external) and Pb 3/4 (internal) probes (3rd line). Introduction of Flp recombinase, achieved by crossing high percentage chimaeras (obtained from blastocyst injection of these ES cells) to C57Bl/6 FLP mice, removed the Neo cassette, leaving exon 18 flanked by loxP sites (4th line). Cre-mediated recombination at these loxP sites deletes exon 18. *Mertk^{fl/fl}* mice, together with PCR-based protocols for their genotyping, are available upon request from the Rothlin laboratory (contact C.V.R.). See Methods for further information.



Extended Data Figure 5 | Persistence of microglial-specific Mer ablation following tamoxifen injection of *Cx3cr1*^{CreER/+}*Mertk*^{fl/fl} mice.

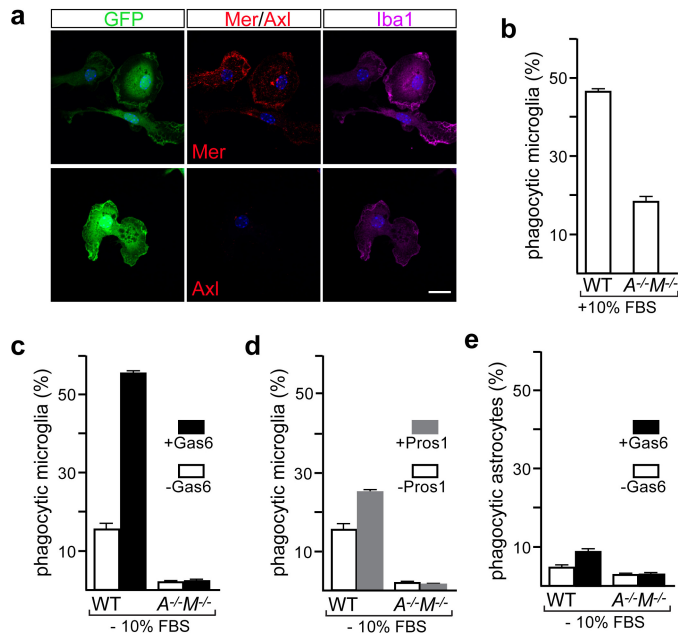
a, Mice were injected intraperitoneally with oil vehicle alone (–tamoxifen, top row) or with tamoxifen (+tamoxifen, bottom row) (see Methods), and brain sections were immunostained for Mer protein expression (red panels in 2nd, 4th columns) in Iba1⁺ microglia (green panels in 1st, 3rd columns) at 1 week (left four panels) and 7 weeks (right four panels)

after injection. Sections counter-stained with Hoechst 33258 to visualize nuclei (blue). **b**, Brain sections containing a brain capillary 7 weeks after injection of vehicle (top) or tamoxifen (bottom), showing that although Mer expression in microglia is eliminated upon tamoxifen-mediated *Cx3cr1*-restricted induction of Cre activity, Mer expression in CD31⁺ microvascular endothelial cells (arrows) is maintained. Representative images of *n* = 2 mice per time point.

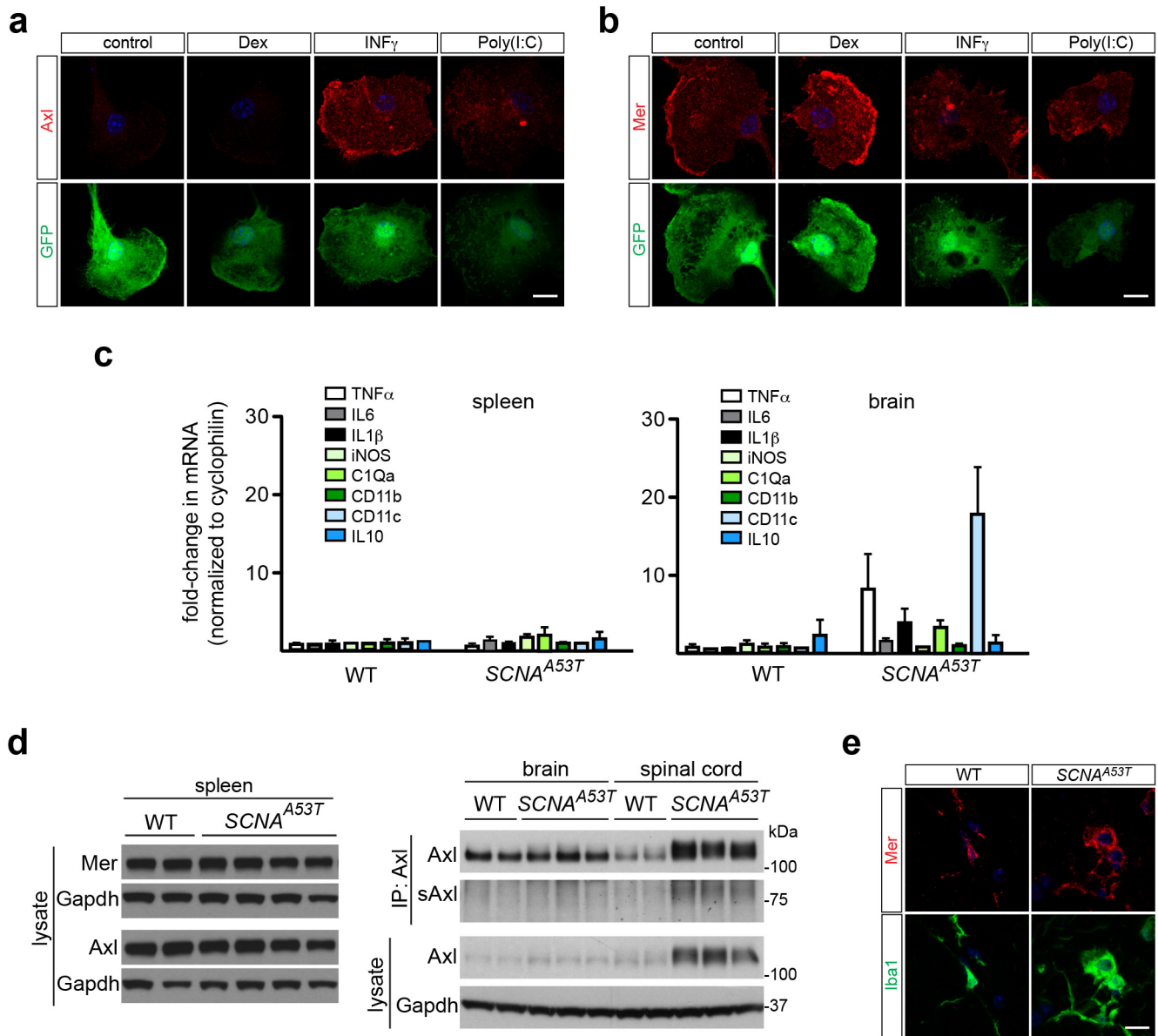


Extended Data Figure 6 | Identity of immigrant BrdU⁺ cells in the olfactory bulb. a, A group of the BrdU⁺ cells in the glomerular layer (gl), visualized 35 days after injection of BrdU (red) and presumed immigrant descendants of SVZ cells in S phase at the time of injection, are also positive for tyrosine hydroxylase (TH, green) in both wild-type (left panel) and *Axl^{-/-}Mertk^{-/-}* (right panel) mice. Arrowheads are examples of

TH⁺BrdU⁺ cells. **b,** Similar comparative granule cell layer (gcl) sections stained with anti-BrdU (red) and calretinin (CR, green). Arrowheads are examples of CR⁺BrdU⁺ cells. Sections were co-stained with Hoechst 33258 to visualize nuclei. Scale bars, 50 μm. Representative images of *n* = 2 per genotype.



Extended Data Figure 7 | Both Gas6 and Pros1 drive microglial phagocytosis of apoptotic cells *in vitro*. **a**, Cultured microglia express Mer but little or no Axl under basal conditions. Microglia were cultured from wild-type $Cx3cr1^{GFP/+}$ mice, visualized for GFP (1st column), and immunostained for Iba1 (3rd column), Mer (2nd column, top), and Axl (2nd column, bottom). Scale bar, 10 μ m. **b–d**, *In vitro* pHrodo-based assay of phagocytosis of apoptotic cells by microglia (see Methods). **b**, In serum-containing medium (10% FBS), wild-type microglia are effective phagocytes; mean phagocytic activity is substantially reduced in $Axl^{-/-}Mertk^{-/-}$ ($A^{-/-}M^{-/-}$) microglia. **c, d**, Both purified Gas6 (**c**) and purified Pros1 (**d**) stimulate AC phagocytosis by cultured microglia in serum-free medium, and this stimulation is entirely TAM-dependent. **e**, The phagocytic activity of cultured astroglia prepared from $Cx3cr1^{GFP/+}$ mice that were either wild-type or $Axl^{-/-}Mertk^{-/-}$ was measured in the same pHrodo-based assay in serum-free medium \pm Gas6. For this FACS-based assay, astrocytes were gated using an astrocyte-specific surface antigen-2 (ACSA-2) antibody (see Methods). Bar graphs represent mean phagocytic activity (\pm s.e.m.); $n = 2$ replicates from 2 mice per genotype (**b–d**), and 2 replicates from 4 mice per genotype (**e**).



Extended Data Figure 8 | Regulation of microglial Axl by neuroinflammation. **a, b,** Axl (**a**) and Mer (**b**) regulation in purified (GFP⁺) cultured microglia by the tolerogenic stimulus dexamethasone (Dex) and the two proinflammatory stimuli IFN γ and poly(I:C), as assessed by immunostaining. Axl expression (**a**) is very low in the absence of an added stimulus, is not elevated by Dex, but is strongly upregulated by both IFN γ and poly(I:C). In contrast, Mer expression (**b**) is readily detected in the absence of an added stimulus, is further elevated by Dex, but is modestly suppressed by both IFN γ and poly(I:C). Scale bar, 10 μ m. **c,** In contrast to the spinal cord (see Fig. 4a), there is no upregulation of the indicated inflammatory mediator/marker mRNAs

(mean expression \pm s.e.m.) in the spleens, and only modest upregulation in the brains, of *SNCA*^{A53T} mice at 8–10 months of age. $n = 3$ mice for each genotype. **d,** Western blot analysis of spleen (left blots) and brain and spinal cord (right blots) extracts from two different wild-type mice and four or three different *SNCA*^{A53T} mice at 9–10 months, for the indicated proteins, with Gapdh as a loading control. Note that soluble Axl ectodomain (sAxl) is upregulated in the *SNCA*^{A53T} spinal cord concomitantly with Axl. **e,** Although Axl is strongly upregulated in Iba1⁺ microglia in the *SNCA*^{A53T} spinal cord (see Fig. 4d), no upregulation of Mer is observed in these same cells. Scale bar, 10 μ m. $n = 2$ wild-type and 3 *SNCA*^{A53T} mice.